Hamming Window applied to Overlapped Subarrays for Broadband Satellite Communications

M. Pellet, G. Goussetis, *Senior Member, IEEE,* J. Mota, *Member, IEEE,* H. Legay, G. Toso, *Fellow, IEEE*, and P. Angeletti, *Senior Member, IEEE*

***Abstract*—The use of Hamming window for tapering the analog beamformed subarrays is investigated in the context of overlapped hybrid beamformed direct radiating array for broadband satellite communication. Whilst this class of antennas can suppress some of the grating lobes associated with conventional non-overlapped arrays, there are still concerns on interference from remaining grating lobes. We discuss how tapering the analog subarray can complement the grating lobe mitigation strategy and demonstrate that a Hamming window offers a simple closed-form implementation leading to significant reduction of interfering signals. Moreover, by virtue of analytical and numerical results, we derive the configuration of the Hamming window tapering that optimizes the trade-off between sidelobe suppression and gain losses in the main lobe.**

***Index Terms*—beamforming, broadband, direct radiating array, multibeam antennas, overlap, satellite communications**

I. Introduction

The transition from broadcast to broadband satellite communications calls for significantly higher capacity and flexibility [1]. Direct Radiating Arrays (DRAs) presents a favorable solution to meet these requirements and are already being deployed in Low Earth Orbit (LEO) constellations. In conventional DRA with Digital Beam Forming Network (DBFN), all the elements are connected to the On-Board Processor (OBP) and active amplifiers [2]. However, to meet the stringent link budget associated with broadband applications from Geostationary Earth Orbit (GEO), thousands of radiating elements are required. Nowadays OBPs can support up to a few hundred ports processing the entire downlink spectrum, a number which is insufficient to address the overall number of required radiating elements. Moreover, full Earth coverage requires thousands of simultaneous beams, which restricts the on-board signal processing capabilities.

To overcome this technological limitation, hybrid beamforming, combining an analogue beamforming network with a digital one, is a promising solution. A common architectural implementation relies on arrays organized in subarrays [3,4]. The analog beamformer processes all the radiating elements within a subarray. The digital OBP, in turn, processes the lattice of subarrays and has now several dozens of elements associated with the ports. In this architecture, the subarrays are seen at digital level as large radiating elements. Because of their large physical dimensions, grating lobes are generated and give rise to unwanted interference. Overlapping strategies is a solution to mitigate totally [11] or reduce the grating lobes [9, 10] while keeping a periodicity and modularity in the architecture, crucial to keep an acceptable manufacturing.

Applying a tapering function in the analog beamforming adopted at subarray is an additional technique to reducing the grating lobes [12]. In [13] nulling control or predictive algorithms [14-15], have been proposed. However, the combination of tapering and overlapping is done through the literature [16-18] with adaptive tapering – often targeting a null in the grating lobe position [19], which is scanning dependent. It implies repeating the nulling process along all desired directions. These techniques are therefore computationally unaffordable for the OBP. Instead, fixed tapering techniques are preferrable for multiple beams generation [20]. They are compatible with recently emerged resource allocation schemes [21], and real-time processing.

There is a gap in the literature in the investigation of fixed optimal tapering functions for overlapped DRAs with respect to multibeam requirements. Widely used in signal processing applications, Hamming windows [22] can be considered; they are related to harmonic analysis [23,24]. They present the advantage of being parametrizable to optimize the cancellation of unwanted lobes. In addition, this tapering is compatible with Fast Fourier Transform (FFT) and hence guarantees fast on-board implementation of the generated beams. In this letter, we propose the use of a Hamming window for the DRA architecture presented in [11]. Ultimately it is shown that wisely parameterizing the window helps reduce grating lobes further at low cost, leading to lower-interference transmissions.

II. General use of the Hamming window

Overlapping subarrays is proceeded with an additional layer of analog devices shifted by half the size of a subarray along the two main Cartesian axes [11]. The beamforming scheme is depicted in Fig. 1. As shown, the radiating elements are fed by either one or two Analog Beam Forming Networks ($ABFNs$),

This paper was submitted in May 2025. This work is supported in part by the European Space Agency under Grant 4000135641/21/NL/GLC /my .

M. Pellet is with Heriot-Watt University, Edinburgh, UK and with Thales Alenia Space, Toulouse, France (e-mail margaux.pellet@thalesaleniaspace.com)

G. Goussetis and J.Mota are with Heriot-Watt University, Edinburgh, UK (e-mail G.Goussetis@hw.ac.uk, J.Mota@hw.ac.uk)

H.Legay is with Thales Alenia Space, Toulouse, France (e-mail herve.legay@thalesaleniaspace.com)

G. Toso, P. Angeletti are with the European Space Agency (esa-ESTEC), Noordwijk, the Netherlands (e-mail Giovanni.Toso@esa.int, Piero.Angeletti@esa.int)

depending on whether they are situated at the edge or center of the overall array. For simplification, the edges are truncated such that all radiating elements are fed by 2 subarrays.

We introduce a DRA architecture comprising 8 × 8 subarrays, each containing 8 × 8 radiating elements (RE). The overlapping configuration is achieved by introducing an interleaved layer of 9 × 9 ABFNs, where each ABFN feeds an 8 × 8 RE subarray. This results in a total radiating aperture consisting of 4096 RE. This antenna is designed for operation at 20 GHz with a radiating element size of 3.2λ, where λ is the wavelength. As per common practice, the dimension of the radiating element is selected such that it maximizes the array gain while keeping any primary grating lobes associated with its dimensions outside the Earth's field of view from a GEO orbit [25, 26]. Although for medium or low orbit constellations (where the scanning range of the antenna can be quite large) the coupling effect between the REs may be significant, the size of the radiating elements in this case lead to a negligible mutual coupling. Mutual coupling can therefore be ignored in the initial design phase.

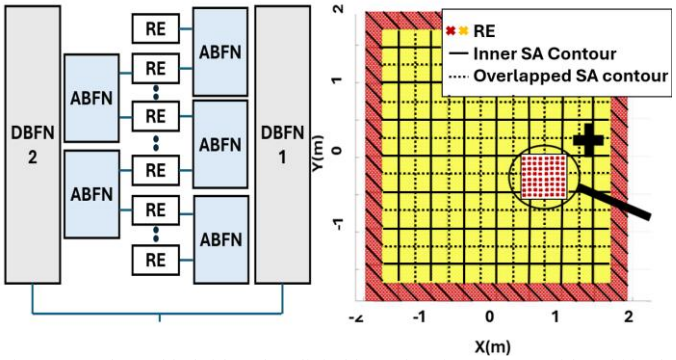

Fig. 1.: Overlapped hybrid analog digital beamforming scheme with a shift of half the size of a subarray (SA) along the two main Cartesian axes. [11]

The Hamming window can be applied either at ABFN or DBFN levels. In theory, the purpose of such window is to mitigate the first side lobe level. In the architecture, the first side lobe level at subarray level is the first order grating lobe. This is illustrated in Fig. 2, where a cosine on a pedestal is represented in a continuous spatial domain (Fig. 2-right) and sampled on the positions of a discrete 8 × 8 planar sub-array (Fig. 2-left). Mathematically, this is described in (1), where $k = 0 \dots n_x - 1$ is the index of the radiating element within the subarray, n_x is the number of RE within a subarray along the x-axis, and d_x is the spacing factor between the RE. The position in the Cartesian domain is denoted as x_k. In the following, the y-axis variables are defined similarly. From (1) the 2-D taper is obtained by a discrete sampling of all coordinates $(x_k, y_k)\ \forall\ k \in [1, n_x], l \in [1, n_y]$ related to their distance to the centre of the subarray.

$$w(x_k) = \alpha + (1-\alpha)\cos\left(\frac{2\pi x_k}{n_x d_x \lambda}\right) \tag{1}$$

The $\alpha \in [0\ 1]$ parameter can be modified for a maximal mitigation of the first side lobe [22]. The value of α depends on the architecture and corresponds to the null of the derivative of the transmitted signal.

Applying the Hamming window at DBFN level would reduce the first side lobe level of the full pattern. It is an unnecessary step which introduces aperture inefficiency, particularly critical for active transmitting arrays for which a high directivity is required. On the contrary, applying the Hamming window at ABFN level corresponds to the cancellation of the first side-lobe generated by the subarray pattern. The grating lobes are included inside these subarray lobes and their levels can be mitigated. This technique therefore guarantees an impact on the unwanted grating lobes in the full pattern. Notwithstanding the tapering at sub-array level, the aperture efficiency remains relatively high due to the overlapping configuration: at nadir, the gain passes from a maximal radiating aperture of 57.21 dB to 57.15 dB. The selection of α is detailed in Section III.

The Fourier transform of the Hamming window is given in (2), where D_A represents the Dirichlet kernels [24] of the ABFN. D_D is the Dirichlet kernel from the DBFN, which size is different from the aforementioned one. The total formulation of the array factor, corresponding to the transmitted signal of a spot beam, is also given in (2). We denote (N_{sub_x}, N_{sub_y}) the number of radiating elements along the Cartesian directions.

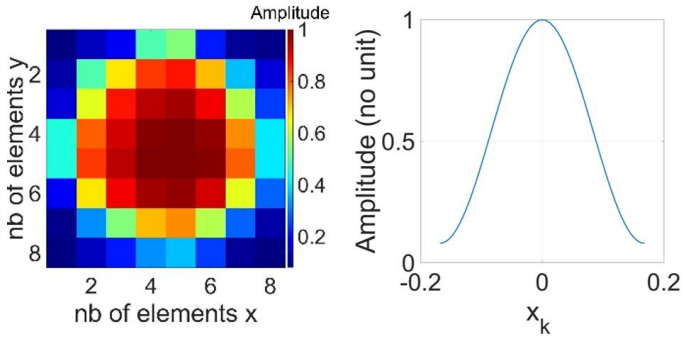

Fig. 2.: Hamming window computed on 64 radiating elements for $\alpha = 0.54$. On the left, cosine on pedestal shape. On the right, 2D distribution.

$$A(u,v) = \frac{1}{N_{sub_x} N_{sub_y}} E(u,v) F(u,v) \left(e^{-j\pi n_x d_x u} + 1\right) D_D(u) \left(e^{-j\pi n_y d_y} + 1\right) D_D(v) \tag{2}$$

with $D_D(u) = \dfrac{\sin(\pi N_{sub_x} n_x d_x u)}{\sin(\pi n_x d_x u)}$,

$$F(u) = \alpha D_A(u) + \frac{(1-\alpha)}{2}\left(D_A\left(u - \frac{1}{d_x n_x}\right) - D_A\left(u + \frac{1}{d_x n_x}\right)\right)$$

and $D_A(u) = \dfrac{\sin(\pi n_x d_x u)}{\sin(\pi d_x u)}$

The amplitude distribution across the overall array is shown in Fig. 3 for $\alpha = 0.54$ for beams pointing at nadir and at $\theta = 1^{o}$. As depicted, cosine pedestals are superposed. Each of them corresponds to the size of a subarray, arranged within an isosceles lattice due to the shift by half the size of a subarray. The sum is observed at the intersection of the subarrays, implying high power levels within a rectangular lattice. The maximum amplitude variation is 9.8 dB in the non-scanned case.

When scanning, the distribution is smoother. Because the uniformity of the power is directly related to the gain, it implies a limited gain loss while scanning. Therefore, the aperture efficiency is maintained. The shift by half the size of a subarray implies a non-coherence between the phases coming from the two ABFN layers that guarantees low amplitude variations, corresponding to the terms $1 + e^{-j\pi n_x d_x}$ and $1 + e^{-j\pi n_y d_y}$ in the formulation in (2).

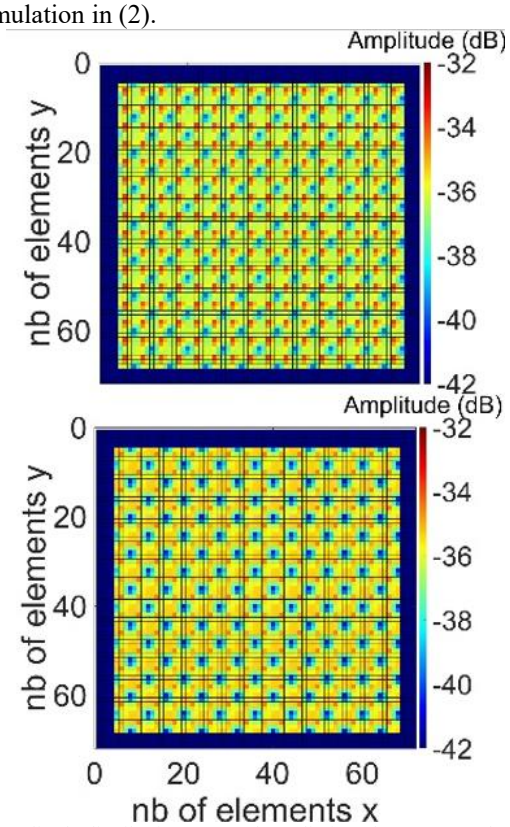

Fig. 3.: Amplitude distribution across the radiating elements. On the left, scan at nadir. On the right, scan at $\theta = 1^o$ along $\phi = 0°$.

III. IMPACT ON THE GRATING LOBE MITIGATION

The improvements brought by the variations of the α parameter are investigated in terms of grating lobe mitigation. The best α guarantees the higher ratio between the gain of the main lobe and the reduction of the grating lobe levels. In the first part, the radiation patterns are shown along a 1D-cut for a first visual representation. In the second part, the best α is selected thanks to a statistical investigation for a large range of pointing directions over the Earth field-of-view.

A. Radiation pattern

Several tapers are generated with different α parameters at ABFN levels from (1). The objective is to assess how each taper overcomes the limitation of even grating lobes. As shown in [11], all odd grating lobes are mitigated for this antenna architecture. A better way to show the even grating lobes consists in scanning along the diagonal $\phi = 45^o$. An example is given for a beam pointing at $\theta = 1°$ from the boresight direction. A first comparison is done between 3 values of α in terms of radiation pattern. The radiation patterns are simulated on Fig. 4 for a $\phi = 45^o$-cut. The subarray pattern is shown when scanning. It is noted that the pattern of the subarray patch changes with the DBFN phase as the amplitude across one subarray changes (Fig. 3).

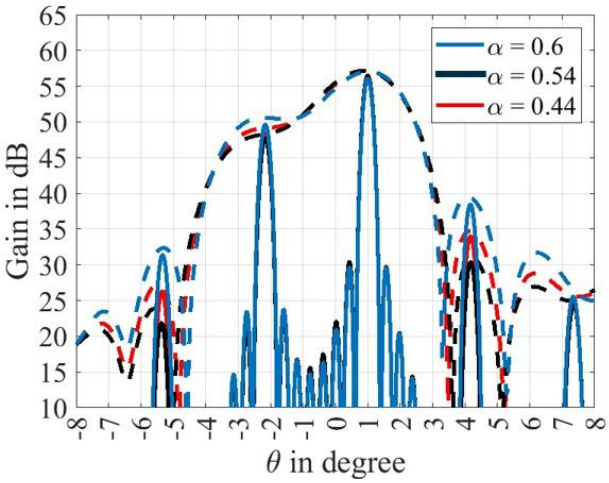

Fig. 4.: Calculated radiation patterns at narrow and broad beam levels for a scan along $\phi = 45°$ at $\theta = 1°$ for a cut..

As shown in Fig. 4, the first grating lobe at –2.1° remains unattenuated. Across the different values of α, variations of approximately 0.5 dB are observed at the main lobe (ML) level and 2 dB for the first grating lobe (GL) levels. The best attenuation, with also the higher gain at ML, occurs for $\alpha = 0.54$ with 47.3 dB versus 49.8 dB and 48.6 dB for $\alpha = 0.6$ and $\alpha = 0.44$ respectively. This behaviour is attributed to the order of the first GL. When the GL is interpreted as a side lobe of the spot beam pattern, its corresponding order becomes –8. As discussed in Section II.A, tapering applied at either the ABFN or DBFN level primarily affects the first side lobe—at the subarray or overall pattern level, respectively. It implies that fixed tapering cannot mitigate fully the first order GL, despite potentially reducing it along some directions. In contrast, a more pronounced effect is observed on the second order GL. Specifically, the GL at –5.5° exhibits a level of 30.8 dB for α = 0.6, decreasing to 22.9 dB for α = 0.54. Here, the superposition of Hamming windows at ABFN creates an attenuation, as shown with the subarray patterns. The best GL reduction is obtained for $\alpha = 0.54$, which implies that the superposition of cosines when scanning creates a favourable pattern that modulates the narrow beams. The trade-off between α and GL suppression is also constrained by the GL situated outside the $\phi = 45^o$-axis.

B. Benchmark on Earth coverage

A technique for benchmarking the efficiency of the different tapers is to simulate the gain coming from the GL and compare it to the gain of the ML. So far, an example of radiation patterns has been given for 4 different α but only shows the GLs in a single cut. In telecommunication applications, the objective is to generate as many beams as possible over the coverage. It is fundamental to limit the overall impact of the GLs that can be seen as interference.

The position of the even grating lobes can be readily defined thanks to the knowledge of classical array factor theory. Deriving the formula from [27, p36], the grating lobes are situated at $(u_0 + \frac{p}{n_x d_x}, p = 1 \dots u_p\ , v_0 + \frac{q}{n_y d_y}, q = 1 \dots v_q)$,

$$\forall(p+q) = 0\ mod(2)$$

where u_p, v_q are the coordinates of the (p,q) GL. One GL is therefore generated within an isosceles lattice with an axis spacing of 2.23°. Given this information, the gain from the ML and the one coming from all GLs can be efficiently compared. The benchmark parameter $G_{\frac{ML}{GL}}$ is defined in (3).

$$G_{\frac{ML}{GL}} = \frac{gain\ ML}{\sum_{i \in FOV} gain\ GL_i} \tag{3}$$

It is noted that the field of view (FOV) from the satellite coincides with the full Earth as seen from a GEO satellite, corresponding to the values $\theta \approx [-8°, 8°]$. The corresponding orders of the grating lobes within the field of view range from -3 to 3. For the calculation of $G_{\frac{ML}{GL}}$, the full lattice of even grating lobes is considered. It accounts for all ϕ -planes and for all $\theta \in [-8°, 8°]$. From this benchmark parameter, the objective function can be defined in 3 steps thanks to the spot beam formulation in (2). Finding the optimal of such function corresponds to the derivation of f as defined in (4). Such function is derivable as a product of C^{∞}-class functions on $]-\infty, +\infty[$. The analytical formulation, not given here for brevity, is a multiplication of $9pq$ sinc functions and cosines depending on either α or $(1-\alpha)$ for f. The defined derivative is dependent on the scanning position and α. The objective function L in (4) is therefore the minimum of the summation of f' on different directions for different α.

$$f_\alpha(u_o, v_o) = \frac{A(u_0, v_o)}{\sum_{p,q \in FOV} A(u_p, v_q)}$$

$$f'_\alpha(u_0, v_0) = \frac{A'(u_0, v_0)}{\sum_{p,q \in FOV} A(u_p, v_q)} + \frac{\sum_{p,q \in FOV} A'(u_p, v_q)\, A(u_0, v_o)}{\left(\sum_{p,q \in FOV} A(u_p, v_q)\right)^2}$$

$$L(\alpha) = \min_{\alpha \in [0\ 1]} \sum_{u_0, v_0 \in FOV} f'_\alpha(u_0, v_0) \tag{4}$$

To proceed with an investigation on the α optimization, the null of f' is calculated with a software tool in MATLAB for every possible (u, v) position in a defined regional beam, as defined in [11]. The process is repeated for 500 values of $\alpha \in [\,0.1\ 1]$ along one single ϕ. The process is done for all $\phi \in [\,0°\ 359°]$ with a 1 degree step and all θ sampled every 0.1° in the regional beam defined in [11] (roughly a lozenge with a side $a = 0.98$). Then, the total is summed and the minimum accounts for the optimal α as per the objective function L. An example calculation of the benchmark parameter (3) is shown in Fig. 5. for $\theta = 1.5°$ along $\phi = 45°$ and $\phi = 20°$.

As depicted along 45 degrees, there is an optimal value of α for which the overall GL level is the lowest compared to the main gain. It corresponds to $\alpha = 0.502$, which is lower than the classical value used for a Hamming window (0.54). In theory, the 0.54 value perfectly mitigates the first side lobe level [13] of the non-overlapped subarray pattern at nadir. It also guarantees that all side lobe levels remain low. Before $\alpha = 0.502$ the tapering effect is strong, which lowers the main gain as well as all the second order GLs. However, larger than 0.502, the taper is closer to a uniform one, and therefore the second order GLs are not attenuated. At the same time, the main gain is maintained compared to the maximum radiating aperture. The decrease of α compared to the 0.54 value (optimal hamming window parameter) is directly related to the overlap: from a reference subarray point of view, the amplitude distribution is changed. The subarray pattern is a result of a power and phase summation coming from the reference layer and the overlapped one. Therefore, although it is impossible to target the 8^{th} side lobe and cancel it with a fixed taper, the best compromise between the ML and the GL is yielded thanks to a favourable reduction of second order GLs.

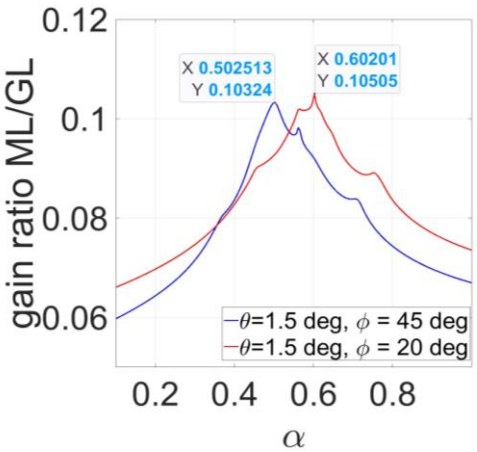

Fig. 5.: Evolution of the ratio between the gain from the ML and the one coming from all the GLs with variations of the α parameter for a scan at $\theta = 1.5°$ along $\phi = 45°$ (blue) and $\phi = 20°$ (red).

As noticed, this best GL mitigation depends on the scanning direction and position. The optimal value is increased along $\phi = 20°$ to 0.602. The calculation of L in (4) gives the best parameter $\alpha = 0.5405$ considering all directions. It matches the optimal Hamming parameter. It means the average amplitude remains unchanged compared to nadir.

Comparatively, Taylor tapers provide GL reduction thanks to SLL targets. When the Taylor taper is applied at ABFN levels, it yields similar GL mitigation principles as the Hamming Window. For such tapers, the sum of $f_\alpha(u_0, v_0)$ over the FoV yielded 33.04 with the optimized SLL target versus a slightly better 33.81 for the Hamming window with $\alpha = 0.5405$. The difference is due to a more controlled broadening of the subarray main lobe with the Hamming window.

This optimal cancellation guarantees a limited interference within the Earth coverage.

IV. Conclusion

A fixed tapering study at analog beamforming level has been conducted in the paper. The use of a Hamming window has been applied to an overlapped hybrid beamformed direct radiating array. The use of such windows leads to a reduced on-board computational complexity. On the other hand, the grating lobe reduction is performed thanks to an optimization of the Hamming Window parameter, reached with $\alpha = 0.5405$. It matches with the one known in the literature as applied to fully digital or fully analog pattern. Using such a taper is critical in telecom systems with thousands of spot beams, enabling interference-limited communication.

V. REFERENCES

[1] R. de Gaudenzi "Challenges in Future Satellite Communications," *IEEE Communication Theory Workshop*, 15 May 2018

[2] P. Angeletti, R. De Gaudenzi, and M. Lisi, "From Bent Pipes to Software Defined Payloads: Evolution and Trends of Satellite Communications Systems," *International Communications Satellite Systems Conferences (ICSSC)*, San Diego (CA), 10-12 Jun. 2008

[3] S. J. Stirland, and A. D. Craig. "Phased arrays for satellite communications: Recent developments at astrium LTD," IET *The Second European Conference on Antennas and Propagation (EuCAP),* pp. 1-5., 2007.

[4] D. Petrolati, P. Angeletti, and G. Toso, "A lossless beam-forming network for linear arrays based on overlapped sub-arrays," *IEEE Transactions on Antennas and Propagation,* Vol. 62, No. 4, 1769-1778, 2013.

[5] M. C. Viganó, G. Toso, G. Caille, C. Mangenot, and I. E. Lager. "Sunflower array antenna with adjustable density taper," *International Journal of Antennas and Propagation*, 2009.

[6] G. Toso, C. Mangenot, and A. G. Roederer, "Sparse and thinned arrays for multiple beam satellite applications," IET *Second European Conference on Antennas and Propagation (EuCAP)*, pp. 1-4., 2007.

[7] P. Rocca, R. J. Mailloux, and G. Toso, "GA-based optimization of irregular subarray layouts for wideband phased arrays design," *IEEE Antennas and Wireless Propagation Letters*Vol. 14, pp. 131-134, 2014.

[8] R. J. Mailloux, S. G. Santarelli, T. M. Roberts, and D. Luu, "Irregular polyomino-shaped subarrays for space-based active arrays," *International Journal of Antennas and Propagation*, 2009.

[9] F. Vidal, H. Legay, G. Goussetis, J-P. Fraysse, "Joint precoding and resource allocation strategies applied to a large direct radiating array for GEO telecom satellite applications," *15th European Conference on Antennas and Propagation (EuCAP)*, 2021.

[10] V. Tugend, and A. Thain, "Hybrid beamforming with reduced grating lobes for satellite applications," *12th European Conference on Antennas and Propagation (EuCAP)*, 2018

[11] M. Pellet, G. Goussetis, H. Legay, J. Mota, B. Cortazar, and G. Toso, "A new antenna array architecture with hybrid beamforming for broadband satellite communications," *17th European Conference on Antennas and Propagation (EuCAP)*, 2023.

[12] M.R. Sarker, M.I. Maynul, M. Tanjilul Alam, and M. Hossam-E-Haider. "Side lobe level reduction in antenna array using weighting function." *IEEE international conference on electrical engineering and information & communication technology*, pp. 1-5., 2014.

[13] J. A. Vásquez-Peralvo, J. Querol, F. Ortíz, J. L. G. Rios, E. Lagunas, V. M. Baeza and S. Chatzinotas: "Flexible beamforming for direct radiating arrays in satellite communications." *IEEE Access,* 2023.

[14] M. A. Almagboul, F. Shu, Y. Qian, X. Zhou, J. Wang and J. Hu: "Atom search optimization algorithm based hybrid antenna array receive beamforming to control sidelobe level and steering the null," *AEU-International Journal of Electronics and Communications*, *111*, 152854, 2019.

[15] L. Yang, K. Wang and H. Sun "A grating lobe suppression method for displaced subarrays using genetic algorithm," *IET Microwaves, Antennas & Propagation*, Vol. 16, No. 7, pp. 457-464, 2022.

[16] J. O. Coleman "Nonseparable Nth-band filters as overlapping-subarray tapers." *IEEE RadarCon (RADAR)*, pp. 141-146., 2011.

[17] R. Haupt, "Reducing grating lobes due to subarray amplitude tapering." *IEEE transactions on antennas and propagation,* Vol. 33, No. 8, pp 846-850, 2003.

[18] J. D. Griesbach "Optimal taper design for overlapped subarray formation." *IEEE Fortieth Asilomar Conference on Signals, Systems and Computers*, pp. 2247-2251, 2006.

[19] X. Ye, Z. Yu, and D. Xiao. "Grating lobe suppression for wideband large-spacing beam scanning array using subarray null adjustable method," *IEEE Antennas and Wireless Propagation Letters,* Vol. 22, No. 2, pp 347-351, 2022.

[20] A. Coskun, S. Cetinsel, I. Kale, R.C. Morling, R. Hughes, S. Brown, and P. Angeletti: "Efficient Coefficient Store in Decomposed DFT/FFT Architectures for On-Board Processors," *31st AIAA International Communications Satellite Systems Conference*, pp. 5710, 2013.

[21] P. Angeletti, R. De Gaudenzi, "Heuristic radio resource management for massive MIMO in satellite broadband communication networks." *IEEE Access*, Vol. 9, pp 147164-14719, 2021.

[22] P. Prajoy, T. Z. Khan, M. H. Khan, and M. M. Rahman, "Comparative performance analysis of hamming, hanning and blackman window," *International Journal of Computer Applications*, Vol. 96, No. 18, 2014.

[23] F. J. Harris, "On the use of windows for harmonic analysis with the discrete Fourier transform," *Proceedings of the IEEE*, Vol. 66, No. 1, pp. 51-83, 1978.

[24] S. Kumar,K. Singh, and R. Saxena, "Analysis of Dirichlet and generalized "Hamming" window functions in the fractional Fourier transform domains," *Signal processing*, Vol. 91, No. 3, pp. 600-606, 2011.

[25] C. G. Christodoulou, Y. Tawk, S. A. Lane, and S. R. Erwin, "Reconfigurable antennas for wireless and space applications," *Proceedings of the IEEE*, Vol. 100, No. 7, pp. 2250-2261, 2012.

[26] C. Stoumpos, J.-P. Fraysse, G. Goussetis, R. Sauleau, and H. Legay,"Quad-furcated profiled horn: The next generation highly efficient geo antenna in additive manufacturing,"*IEEE Open J. Antennas Propag*.,vol. 3, pp. 69–82, 2022

[27] R. J. Mailloux, *Phased array antenna handbook*, Artech house, 2017.